Neutron Reflectometry Study of Solid Electrolyte Interphase Formation in Highly Concentrated Electrolytes

small structures
www.small-structures.com

Neutron Reflectometry Study of Solid Electrolyte Interphase Formation in Highly Concentrated Electrolytes

Josef Rizell, Anton Zubayer, Matthew Sadd, Filippa Lundin, Nataliia Mozhzhukhina, Fredrik Eriksson, Jens Birch, Alexei Vorobiev, Shizhao Xiong, and Aleksandar Matic**

Highly concentrated electrolytes have been found to improve the cycle life and Coulombic efficiency of lithium metal anodes, as well as to suppress dendrite growth. However, the mechanism for these improvements is not well understood. Partly, this can be linked to the difficulty of accurately characterizing the solid electrolyte interphase (SEI), known to play an important role for anode stability and stripping/plating efficiency. Herein, in situ neutron reflectometry is used to obtain information about SEI formation in a highly concentrated ether-based electrolyte. With neutron reflectometry, the thickness, scattering length density (SLD), and roughness of the SEI layer formed on a Cu working electrode are nondestructively probed. The reflectivity data point to the formation of a thin (5 nm) SEI in the highly concentrated electrolyte (salt:solvent ratio 1:2.2), while a considerably thicker (13 nm) SEI is formed in an electrolyte at lower salt concentration (salt:solvent ratio 1:13.7). Further, the SEI formed in the electrolyte with high salt concentration has a higher SLD, suggesting that the chemical composition of the SEI changes. The results from neutron reflectometry correlate well with the electrochemical data from SEI formation.

1. Introduction

With a high theoretical capacity ($3860\ mAh\ g^{-1}$) and low reduction potential (-3.04 V vs standard hydrogen electrode), lithium (Li) metal anodes offer a promising route toward high energy density batteries.[1,2] However, the practical realization of lithium metal batteries has so far been hindered by insufficient Coulombic efficiency (CE) and safety problems, which are directly related to the connected issues of inhomogeneous lithium plating/stripping and the formation of unstable or inhomogeneous solid–electrolyte interphases (SEIs).[3] The SEI plays a central role for metal anodes, both to prevent side reactions[4] and to control the deposition morphology.[5] For instance, an uneven interfacial resistance over the SEI results in preferential growth and a mechanically weak or inflexible SEI can be fractured by the growth of lithium, creating deposition hotspots.[6] Further, inhomogeneously deposited lithium will form low-density mossy structures with a large surface area and a larger electrolyte decomposition as a result. It can also form dendrites which can grow through the separator to short-circuit the cell, or cause capacity loss due to the formation of "dead" lithium.

To enhance the reversibility of lithium metal plating and stripping, several electrolyte modification strategies have been proposed, which often aim to form better SEIs. For instance, numerous salt-solvent combinations and additives have been proposed.[7] In particular, salt concentrations exceeding the conventional $1\ mol\ dm^{-3}$, so-called highly concentrated electrolytes (HCEs), have enabled both stable cycling and uniform plating of lithium.[8,9] Explanations for this improved performance can be divided into two main categories: 1) Li^+-ion depletion at the electrode surface, known to cause dendritic growth, is mitigated when the salt concentration is increased.[8,10] 2) Better SEI layers form when the salt concentration is increased.[11–14] Yet, it is not well understood how the properties of the SEI change with salt concentration.

To characterize the SEI, a host of different techniques has been used. For instance, X-Ray photoelectron spectroscopy (XPS) and Fourier-transform infrared spectroscopy (FTIR) are commonly employed to study the chemical composition,[15] and lately cryo-transmission electron microscopy (TEM) has also allowed imaging of the SEI.[16,17] However, accurate

J. Rizell, M. Sadd, F. Lundin, N. Mozhzhukhina, S. Xiong, A. Matic
Department of Physics
Chalmers University of Technology
41296 Göteborg, Sweden
E-mail: shizhao.xiong@chalmers.se; matic@chalmers.se

A. Zubayer, F. Eriksson, J. Birch
The Department of Physics, Chemistry and Biology
Linköping University
58183 Linköping, Sweden

A. Vorobiev
Department of Physics and Astronomy
Uppsala University
75120 Uppsala, Sweden

A. Vorobiev
Institute Laue-Langevin
38042 Grenoble (Cedex 9), France

The ORCID identification number(s) for the author(s) of this article can be found under https://doi.org/10.1002/sstr.202300119.

DOI: 10.1002/sstr.202300119

experimental characterization of the electrode/electrolyte interface is challenging in a number of ways. For instance, several of the common components of the SEI are known to be very sensitive to air exposure or various contaminations.[15] Further, sample preparation steps after a cycling experiment, such as washing the electrode with solvent to get rid of salt precipitates, can also modify the state of the SEI.[18] Therefore, it has been recognized that in situ analysis is essential to better understand the properties of the SEI.[19] The nanoscale thickness of the SEI further complicates measurements, for instance, by requiring very high resolution for direct imaging. When such images are obtained using electron transmission microscopy, the field of view is limited; usually it is in the range of 10–100 nm.[17,20–22]

To obtain representative information from a larger area of the electrode, ellipsometry[23] and reflectivity measurements have been employed.[24–26] Both X-Ray[24,25] and neutron reflectivity (NR)[26] can be used to perform in situ characterization of the SEI. The weak interaction between neutrons and matter allows the SEI layer to be studied nondestructively and the large penetration depth of neutrons facilitates the use of in situ electrochemical environments. Additionally, isotopic contrast can be utilized with neutrons,[26] allowing high sensitivity to light elements such as Li, which are more difficult to detect in X-Ray experiments, and to optimize the contrast through deuteration of different components.[27–29]

NR has previously been used to study SEI layers formed on Si,[30] carbon,[31,32] and inert substrates like Cu[28] or W.[27,33] In these works, carbonate-based electrolytes with salt concentrations up to 1M were used. Here, we investigate SEI formation in a highly concentrated, ether-based electrolyte using in situ neutron reflectometry and electrochemical characterization. We demonstrate that an increased salt concentration results in a thinner SEI with a lower roughness and a higher scattering length density (SLD), suggesting a change in composition of the SEI. The neutron reflectometry results are correlated to the electrochemical response during SEI formation which reveal a much lower total charge (integrated current) during SEI formation in the highly concentrated electrolyte, in agreement with the formation of a thinner SEI.

2. Neutron Reflectometry Method

In a reflectometry experiment, the reflectivity, i.e., the intensity ratio between an incident and reflected beam, is monitored for different momentum transfer vectors, **Q**. To study the SEI formation using neutron reflectometry, we built a cell where the counter electrode (CE) is a Li foil and the working electrode (WE) is a single-crystal silicon (Si) block, covered first with an adhesion layer of titanium (Ti) and then a 50 nm-thick copper (Cu) film (**Figure 1**a and S1, Supporting Information). The neutron beam enters the cell through the side of the silicon block, which is effectively neutron transparent, to probe the interface between WE and electrolyte from beneath.

In the experiment, the specular reflectivity is measured, i.e., the incident and reflected angles are the same, yielding a typical reflectivity curve as shown in Figure 1b. A fringe pattern, called Kiessig fringes,[34] appears when neutrons reflected at different interfaces in the sample interfere constructively or destructively and thus encode information about different layers. The reflection and transmission of the neutron beam are determined by the neutron SLD of the different layers and thus, to aid the

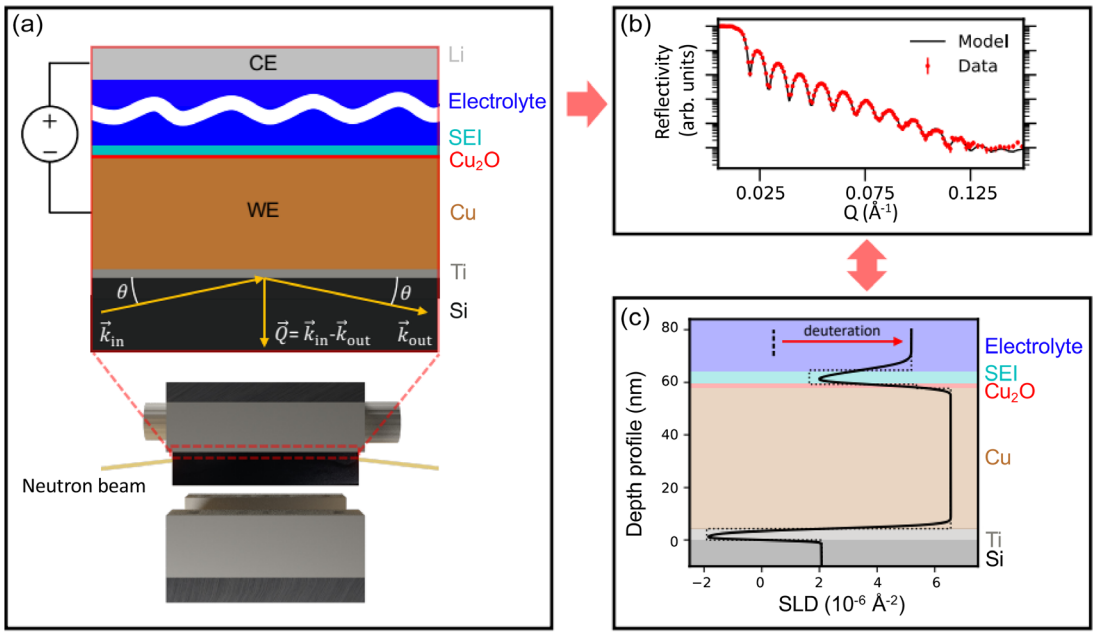

Figure 1. In situ characterization of SEI using neutron reflectometry. a) Beam path through the neutron reflectometry cell and schematic illustration of the electrodes and interfacial layers. b) Typical reflectivity profile. c) Slab model of nanosized layers on top of the Si block. Thicknesses and SLDs of different slabs and the roughness between them are optimized to find a model consistent with the reflectivity data (see text). Dashed line represents the SLD of nondeuterated electrolyte and the dotted line reflects a model without any interfacial roughness.

interpretation of the reflectivity data, a model for the SLD along the depth profile of the sample (Figure 1c) can be fitted to the reflectivity curve. From the fitted SLD profile, information about the composition, thickness, and roughness of layers at the electrode interface can be determined. To optimize the sensitivity for the SEI layer in the NR experiment, the electrolyte is prepared using a fully deuterated solvent with the aim to match the SLD of the electrolyte as closely as possible to the SLD of the substrate (Cu). The change in SLD due to deuteration is visualized in Figure 1c, where the SLD of the nondeuterated electrolyte is shown as a dashed line. The increase in electrolyte SLD by deuteration will enhance changes of the reflectivity curve when an SEI layer is formed.

To obtain as much information as possible about the SEI from the measurements, it is also critical to ensure that the layers sputtered on the Si block have uniform thickness across the entire surface area. A varying thickness will yield a measurement where the observed reflectivity curve is a result of many overlapping fringes with different periods, vastly complicating data analysis. To avoid this, a thickness variation of less than 2% is usually acceptable. Further, more information can be obtained from a measurement on a smooth substrate compared to a rougher one. For a successful experiment, as a rule of thumb, a roughness of around <2 nm (root mean squared value) is required.[35] This relates to a steeper falloff of the reflectivity with Q for more rough samples, yielding a poor signal-to-noise ratio in the measurements. To obtain both smooth and uniformly thick electrodes, the thin films of Ti and Cu covering the Si block were prepared using magnetron sputter deposition. Reflectivity curves from two different as-deposited substrates in a beam-from-air configuration are shown in **Figure 2**. A series of Kiessig fringes is clearly visible well below $Q = 0.1$ Å^{-1}, indicating that the prepared substrates were both uniform in thickness and had adequate surface roughness for the experiment. Additionally, the overlap of the reflectivity curves for the substrates used for the different electrolytes indicates that they have very similar properties and potential changes in the reflectivity curves when the substrates are exposed to the different electrolytes are thus directly a result of SEI formation and not substrate variations.

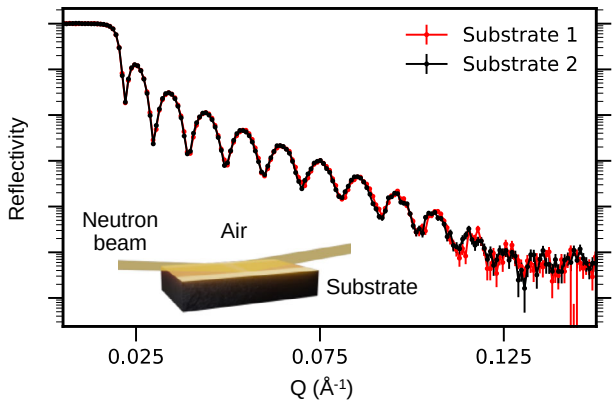

Figure 2. NR curves of the as sputtered substrates measured in a beam-from-air configuration.

3. Results and Discussion

The reduction potentials of the reactions involved in the SEI formation on Cu using electrolytes with low (LCE) and high salt concentrations (HCE) were investigated using cyclic voltammetry (CV) in Li–Cu coin cells (**Figure 3**a). Using a slow scan rate (1 mV s^{-1}), the cathodic scan reveals several peaks between 0.4 and 1.2 V versus Li/Li$^+$, corresponding to the electrochemical reduction of different electrolyte species at the Cu surface.[36] In this voltage range, the conversion of the oxide layer covering the electrode to Cu and Li_2O should also take place.[37,38] A steep increase in the current below 0 V versus Li/Li$^+$ arises when metallic Li is deposited on the Cu surface. Conversely, the first peak in the anodic scan marks Li stripping, while the lack of other oxidative peaks until 1.2 V suggests that most of the electrolyte reduction processes that were observed during the anodic scan are irreversible.

To form a self-passivating SEI on a Cu electrode, a potentiostatic hold at 50 mV versus Li/Li$^+$ was applied. This potential is low enough that all decomposition reactions observed in the CV (Figure 3a) can occur in parallel while Li deposition is avoided. When this potentiostatic hold is applied in a fresh Li–Cu cell, a large current is initially observed, which quickly decays as the SEI layer passivates the electrode (Figure 3b). After 15 min, the current density has dropped to less than 0.01 mA cm^{-2} for both electrolytes, more than three orders of magnitude smaller than the peak current (Figure S2, Supporting Information). One can note that the maximum current density during the potentiostatic hold is considerably lower with the HCE compared to the LCE, indicating that less electrolyte decomposition occurs at the higher salt concentration.

The results from the NR experiments are shown in **Figure 4**a. At OCV, the reflectivity curves from the WE in both the LCE and HCE show characteristic Kiessig fringes. To aid the interpretation of the reflectivity data, a model for the SLD profile at the electrode–electrolyte interface is fitted to the data using a Markov Chain Monte Carlo (MCMC)-based algorithm. Based on knowledge of how the cell was prepared, the Si substrate, Ti and Cu layers sputtered on the Si block, a copper oxide layer which was expected to form due to air exposure of the sputtered copper, as well as the bulk electrolyte, are included in the model. However, this is not sufficient to get an acceptable fit of the model to the reflectivity data at OCV conditions (see Figure S3, Supporting Information). Instead, the model had to include a surface layer with a different SLD on top of the working electrode to obtain a satisfactory fit to the data (Figure 4b,c, S4 and S5, Supporting Information). This could either reflect a surface structure of the liquid, like an electric double layer (EDL),[39,40] or indicate that a chemical reaction has taken place to form this surface layer. In the HCE, the fits to the data suggest that the thickness of this layer is around 2 nm, which is a reasonable thickness for an EDL whereas the corresponding layer in the LCE was close to 8 nm, pointing more toward a chemical reaction(s) taking place already at OCV in this electrolyte (Figure 4d).

After a potentiostatic hold is applied, the fringe amplitude changes, and the positions of some fringe maxima shift (Figure 4a). To account for the differences between the reflectivity curves, the parameters for the outer layers in the model, the Cu_2O and SEI, were allowed to change in response to the

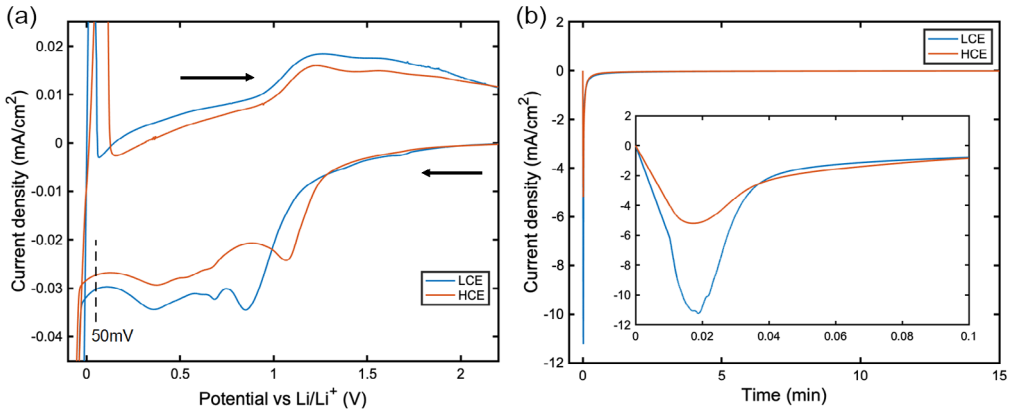

Figure 3. Electrochemical SEI formation in Li–Cu coin cells with electrolytes with low (LCE) and high salt concentrations (HCE). a) CV scans at a 1 mV s^{-1} scan rate. b) Potentiostatic SEI formation at 50 mV versus Li/Li^+.

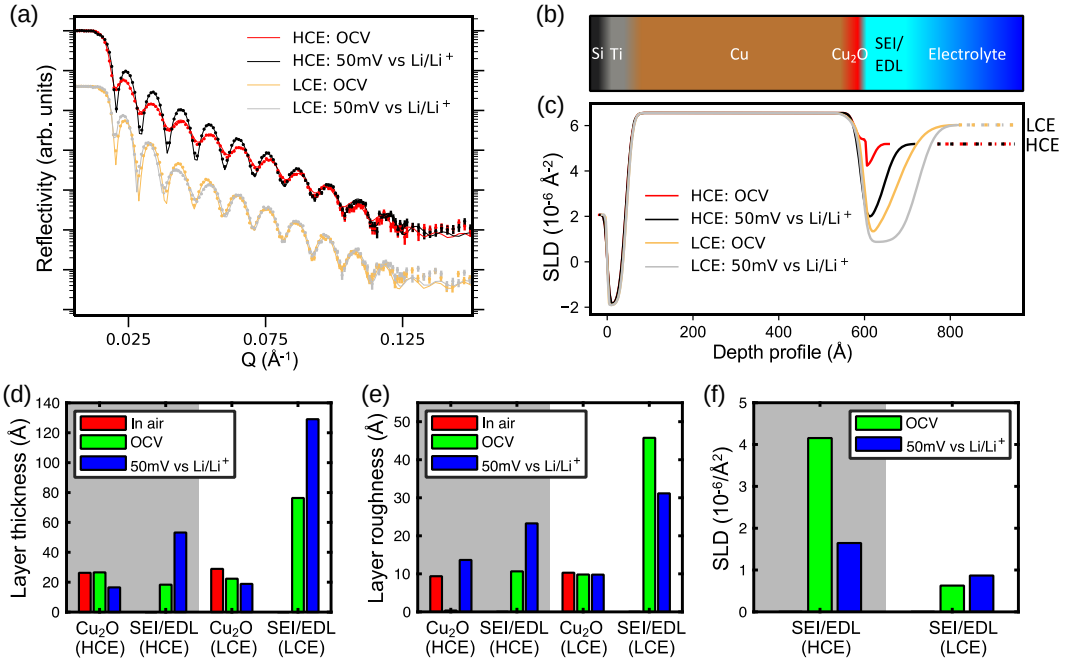

Figure 4. Reflectivity measurements and fits. a) Reflectivity curves obtained in the in situ cell at OCV and during a potentiostatic hold at 50 mV versus Li/Li^+ for LiTFSI/DME electrolytes with high (HCE) and low (LCE) salt concentrations, respectively. Error bars are shown as vertical lines and model fits are marked by solid lines. b) Illustration of the slab model used to fit the data. c) SLD profiles fitted from the reflectivity curves. d) Fitted layer thicknesses of the outer layers. e) Fitted layer roughnesses for the outer layers. f) SLDs of the SEI/EDL formed in the two different electrolytes.

potentiostatic hold. The fitted SLD profiles (Figure 4c) suggest that changes in the reflectivity curve after the potentiostatic hold can be explained by the formation of an SEI layer with a lower SLD than the bulk electrolyte (Note S1, Supporting Information). The fitted models show that the reflectivity data are consistent with an SEI thickness of 5 nm for the HCE and 13 nm for the LCE (see Figure 4d). This corresponds well to SEI thicknesses found with cryo-TEM, typically ranging from 10 to 20 nm.[17,22] Figure 4e shows that the interfacial roughness of the SEI layer formed after the potentiostatic hold is higher for the LCE (3.1 nm) compared to the HCE (2.3 nm), which can be a sign that a more homogenous SEI is obtained in the HCE. The roughness reported here should be interpreted as a local average of the thickness of the interface region between two materials and corresponds to a sloping part of the SLD profile. It can be both a well-defined, but tortuous, boundary between two materials and/or a region of interdiffusion.[41] Reflectometry measurements effectively measure the sample structure averaged over in-plane inhomogeneities smaller than the coherence length of the beam, ≈1 μm $(\sin\theta)^{-1}$, where θ corresponds to the grazing incidence angle of the beam.[35] Here, with a maximum incidence angle of 8°, we effectively measure the average structure of all inhomogeneities <10 μm. The fits also indicate that the SEI formed in the HCE has a higher SLD than the SEI formed in the

LCE (Figure 4f), pointing toward a different composition and/or a different density/porosity of the SEI formed in the two electrolytes. One can speculate that the increased SLD could be a result of more inorganic components in the SEI, but to firmly conclude this further investigations would be needed.

In the fitting process using the MCMC-based algorithm, the parameter space of the defined model is sampled. By analyzing the points in parameter space that the algorithm visits, additional information about the fit can be gathered (Figure S6–S9, Supporting Information). For instance, the slab model used here for the SEI creates some interdependence between the SEI roughness, thickness, and SLD. This parameter entanglement is seen in the MCMC fit, as a partial correlation between these parameters (Figure S5 and S6, Supporting Information). Further, Figure S5 and S6, Supporting Information, show that the Cu_2O thickness and Cu thickness are anticorrelated, meaning that the thickness of each layer cannot be reliably decoupled from the NR fit. The fitted parameters from the SLD profile suggest that the Cu_2O thickness changes after adding electrolyte in the cell and after applying the potentiostatic step. In part, this might reflect actual changes of the oxide layer thickness in response to the applied potential;[38] however, it is also possible that the similarity in SLD between this layer and bulk Cu makes it difficult to reliably assert the thickness independently. Still, the thicknesses assigned to the Cu_2O layer in these measurements are in agreement with the literature, where Cu exposed to air at ambient temperature has been reported to form oxide layers that are 20–50 Å thick.[42]

The NR measurements offer a unique opportunity to probe and compare SEI layers formed in different electrolytes in situ. To further increase the information which can be obtained on the SEI layer, contrast optimization of the SLD profiles through careful selection of substrate materials and/or varying the electrolyte deuteration are promising routes.[33] Ideally, for optimal contrast all materials in the cell (substrate, electrode, electrolyte) should have the same SLD, different from the formed SEI.[35] That way, the reflectivity curve carries features only from the SEI. This can allow more advanced models of the SEI to be reliably fitted to the reflectometry data. Further, modern neutron focusing optics and new neutron sources can allow cells with electrode sizes more similar to coin cells to be used, while measurement times are reduced.[43]

4. Conclusion

Using in situ NR measurements, we observed that at OCV, certain surface structure is created on the Cu electrode, either through chemical reactions or by forming an electric double layer. The nature of this layer depends on the salt concentration in the electrolyte, where a HCE has a thinner layer with higher SLD than the LCE. As a potentiostatic hold at 50 mV versus Li/Li^+ is applied, the electrochemical SEI formation can be triggered and detected with the NR. The reflectivity data are consistent with the formation of a thinner, and potentially more homogenous, SEI in the HCE compared to the LCE. The higher SLD of the SEI formed in the HCE reflects a change in composition, e.g., a more inorganic components, and/or porosity. This is an important finding to understand how increasing the electrolyte salt concentration affects the SEI formation, especially in anode-free lithium metal cells or Li–Cu cells. More broadly, this study highlights the possibility of comparing the SEI layers formed in different electrolytes and on different substrates using in situ NR measurements.

5. Experimental Section

Electrolyte Preparation: 1,2-Dimethoxyethane (DME) (Sigma–Aldrich, 99.4% deuteration and nondeuterated) was dried over molecular sieves and filtered through a syringe filter. Lithium bis(trifluoromethanesulfonyl)imide (LiTFSI) (Solvionic) was dried at 80 °C in vacuum for 72 h. The dried salt and solvent were mixed in molar ratios (LiTFSI:DME) of 1:2.2 (HCE, 2.8 M) and 1:13.7 (LCE, 0.66 M) and magnetically stirred for 24 h at room temperature to ensure complete dissolution of the salt.

In Situ Cell: A closed electrochemical cell (Figure S1a, Supporting Information) was constructed, wherein a Si substrate coated with a thin Cu layer (≈50 nm thick) was used as the working electrode. The electric contact with the Cu electrode was made at three points using gold springs mounted on a brass plate (see Figure S1b, Supporting Information). A rubber *o*-ring was pressed against the Cu surface to keep the cell airtight, and the active working electrode area was 25.07 cm^2. The counter electrode was a Li metal foil (200 μm thick). The distance between the electrodes was 0.5 mm, defined by two PEEK spacers placed in diagonal corners of the cell.

Single-crystal Si blocks (Sil'tronix, 50 × 80 × 15 mm) polished to <0.5 nm nominal rms surface roughness were sonicated: first in acetone and then in isopropanol and finally blown dry with N_2 gas. Sputtering of the Ti and Cu layers was carried out using a Ceme Con (Coatings, Technology & Process) CC800/9 ML magnetron sputtering system.

Neutron Reflectometry: NR experiments were performed at the SuperADAM reflectometer at Institut Laue-Langevin. The reflectivity was probed in the Q_z range 0–0.32 $Å^{-1}$ by rotating the sample to change the incidence angle of the monochromatic neutron beam, $\lambda = 5.21$Å. The intensity of the reflected beam was detected using a 30 × 30 cm^2 2D ^{3}He position-sensitive detector. The measurement time was around 3 h.

First, the Si substrate was characterized in a "beam-from-air" configuration to determine the layer parameters associated with the substrate. Subsequently, measurements with the substrates in the neutron reflectometry cell filled with electrolyte were carried out both at OCV and 15 min after starting a potentiostatic hold at 50 mV versus the Li counter electrode.

Data were reduced using the software pySAred. In the data reduction process, the beam was normalized using the total reflection plateau. At low incidence angles, the incident beam was larger than the substrate, and to account for this, an over illumination correction, or "footprint" correction, was applied.[44]

To aid the data interpretation, a slab model for the depth profile of the sample was constructed and fitted to the data. Each layer in the model was assigned a thickness, a neutron SLD, and a roughness (expressed as a Gaussian profile). These model parameters were fitted using the DiffeRential Evolution Adaptive Metropolis (DREAM) MCMC algorithm in the software Refl1D.[45] From these fits, the uncertainties of the fitted parameters in the model could be estimated.

The SLD profiles for all measurements on the same substrate were refined simultaneously to find a suitable model to describe the layers on the surface of the Si block (Figure S4 and S5, Supporting Information). The model included six different layers: Si, Ti, Cu, Cu_2O, a layer representing the SEI/EDL, and bulk electrolyte with an interfacial roughness between each layer. The parameters of the inner layers (Si, Ti, Cu) were kept constant for all measurements on the same substrate as they were not expected to change by adding the electrolyte or applying a potential across the cell, while the Cu_2O and SEI/EDL layers were allowed to change to account for the changes in the reflectivity curves. However, to limit the number of parameters fitted, the materials Si, Ti, Cu, Cu_2O, and electrolyte were fixed to their bulk SLDs (see Table S1, Supporting

Information). The bulk SLD of the deuterated electrolytes was calculated based on their composition and density measurements carried out with an Anton Paar DMA 4500 M density meter. All parameters fitted are listed in Table S2, Supporting Information, and histograms of the parameter values for all points visited in the MCMC fit are shown in Figure S7 and S8, Supporting Information.

Electrochemical Measurements: Both coin cells and reflectivity cells were assembled inside an argon-filled glove box. Coin cells were assembled with a Li-metal foil (Hanjo metal, 200 µm thick, 10 mm diameter) as a counter electrode, a Whatman 2400 separator (16 mm diameter), a copper foil (13 mm diameter, Goodfellow) as the working electrode and with 40 µL of electrolyte. The cells were controlled using a BioLogic potentiostat. For the cyclic voltammograms, the scan rate was 1 mV s^{-1} and the potentiostatic hold was applied at 50 mV versus the lithium counter electrode for 15 min.

Supporting Information

Supporting Information is available from the Wiley Online Library or from the author.

Acknowledgements

The authors acknowledge Grzegorz Greczynski for kindly providing us access to use his magnetron sputtering system and the Swedish research council for funding the national infrastructure Super ADAM. FORMAS and VINNOVA competence center BASE are acknowledged for funding the research. J.B. is grateful for support from the Swedish Government Strategic Research Area in Materials Science on Advanced Functional Materials (AFM) at Linköping University (Faculty Grant SFO Mat LiU No. 2009 00971), F.E., A.Z., and J.B. thank the Swedish Science Council for support through the project "Isotope-enriched boron carbide containing amorphous multilayer neutron optics" (VR 2019-04837).

Conflict of Interest

The authors declare no conflict of interest.

Data Availability Statement

The data that support the findings of this study are available from the corresponding author upon reasonable request.

Keywords

highly concentrated electrolytes, lithium metal anodes, neutron reflectometry, solid electrolyte interphase, thickness

Received: March 31, 2023
Revised: June 20, 2023
Published online:

[1] D. Lin, Y. Liu, Y. Cui, *Nat. Nanotechnol.* **2017**, *12*, 194.
[2] J. Liu, Z. Bao, Y. Cui, E. J. Dufek, J. B. Goodenough, P. Khalifah, Q. Li, B. Y. Liaw, P. Liu, A. Manthiram, Y. S. Meng, V. R. Subramanian, M. F. Toney, V. V. Viswanathan, M. S. Whittingham, J. Xiao, W. Xu, J. Yang, X. Q. Yang, J. G. Zhang, *Nat. Energy* **2019**, *4*, 180.
[3] J. G. Zhang, W. Xu, J. Xiao, X. Cao, J. Liu, *Chem. Rev.* **2020**, *120*, 13312.
[4] E. Peled, *J. Electrochem. Soc.* **1979**, *126*, 2047.
[5] K. N. Wood, M. Noked, N. P. Dasgupta, *ACS Energy Lett.* **2017**, *2*, 664.
[6] F. Hao, A. Verma, P. P. Mukherjee, *J. Mater. Chem. A Mater.* **2018**, *6*, 19664.
[7] W. Xu, J. Wang, F. Ding, X. Chen, E. Nasybulin, Y. Zhang, J. G. Zhang, *Energy Environ. Sci.* **2014**, *7*, 513.
[8] X. Xu, Y. Liu, J.-Y. Hwang, O. O. Kapitanova, Z. Song, Y.-K. Sun, A. Matic, S. Xiong, *Adv. Energy Mater.* **2020**, *10*, 2002390.
[9] J. Qian, W. A. Henderson, W. Xu, P. Bhattacharya, M. Engelhard, O. Borodin, J. G. Zhang, *Nat. Commun.* **2015**, *6*, 6362.
[10] J. N. Chazalviel, *Phys. Rev. A* **1990**, *42*, 7355.
[11] J. Zheng, J. A. Lochala, A. Kwok, Z. D. Deng, J. Xiao, *Adv. Sci.* **2017**, *4*, 1700032.
[12] B. Liu, W. Xu, P. Yan, S. T. Kim, M. H. Engelhard, X. Sun, D. Mei, J. Cho, C. M. Wang, J. G. Zhang, *Adv. Energy Mater.* **2017**, *7*, 1602605.
[13] S. K. Jeong, H. Y. Seo, D. H. Kim, H. K. Han, J. G. Kim, Y. B. Lee, Y. Iriyama, T. Abe, Z. Ogumi, *Electrochem. Commun.* **2008**, *10*, 635.
[14] X. Fan, L. Chen, X. Ji, T. Deng, S. Hou, J. Chen, J. Zheng, F. Wang, J. Jiang, K. Xu, C. Wang, *Chem* **2018**, *4*, 174.
[15] P. Verma, P. Maire, P. Novák, *Electrochim. Acta* **2010**, *55*, 6332.
[16] J. Wang, W. Huang, A. Pei, Y. Li, F. Shi, X. Yu, Y. Cui, *Nat. Energy* **2019**, *4*, 664.
[17] Y. Li, Y. Li, A. Pei, K. Yan, Y. Sun, C. L. Wu, L. M. Joubert, R. Chin, A. L. Koh, Y. Yu, J. Perrino, B. Butz, S. Chu, Y. Cui, *Science* **2017**, *358*, 506.
[18] S. T. Oyakhire, H. Gong, Y. Cui, Z. Bao, S. F. Bent, *ACS Energy Lett.* **2022**, *7*, 2540.
[19] A. M. Tripathi, W. N. Su, B. J. Hwang, *Chem. Soc. Rev.* **2018**, *47*, 736.
[20] M. Dollé, S. Grugeon, B. , L. Dupont, J. M. Tarascon, *J. Power Sources* **2001**, *97–98*, 104.
[21] W. Huang, P. M. Attia, H. Wang, S. E. Renfrew, N. Jin, S. Das, Z. Zhang, D. T. Boyle, Y. Li, M. Z. Bazant, B. D. McCloskey, W. C. Chueh, Y. Cui, *Nano Lett.* **2019**, *19*, 5140.
[22] Z. Zhang, Y. Li, R. Xu, W. Zhou, Y. Li, S. T. Oyakhire, Y. Wu, J. Xu, H. Wang, Z. Yu, D. T. Boyle, W. Huang, Y. Ye, H. Chen, J. Wan, Z. Bao, W. Chiu, Y. Cui, *Science* **2022**, *375*, 66.
[23] F. Kong, F. McLarnon, *J. Power Sources* **2000**, *89*, 180.
[24] C. Cao, T. P. Pollard, O. Borodin, J. E. Mars, Y. Tsao, M. R. Lukatskaya, R. M. Kasse, M. A. Schroeder, K. Xu, M. F. Toney, H.-G. Steinrück, *Chem. Mater.* **2021**, *33*, 7315.
[25] T. Kawaguchi, K. Shimada, T. Ichitsubo, S. Yagi, E. Matsubara, *J. Power Sources* **2014**, *271*, 431.
[26] Ye. N. Kosiachkin, I. v. Gapon, A. A. Rulev, E. E. Ushakova, D. Merkel, L. A. Bulavin, M. v. Avdeev, D. M. Itkis, *J. Surf. Invest: X-Ray, Synchrotron Neutron Tech.* **2021**, *15*, 787.
[27] C. H. Lee, J. A. Dura, A. LeBar, S. C. DeCaluwe, *J. Power Sources* **2019**, *412*, 725.
[28] J. E. Owejan, J. P. Owejan, S. C. Decaluwe, J. A. Dura, *Chem. Mater.* **2012**, *24*, 2133.
[29] M. v. Avdeev, A. A. Rulev, E. E. Ushakova, Y. N. Kosiachkin, V. I. Petrenko, I. v. Gapon, E. Y. Kataev, V. A. Matveev, L. v. Yashina, D. M. Itkis, *Appl. Surf. Sci.* **2019**, *486*, 287.
[30] B. Jerliu, E. Hüger, M. Horisberger, J. Stahn, H. Schmidt, *J. Power Sources* **2017**, *359*, 415.
[31] H. Kawaura, M. Harada, Y. Kondo, H. Kondo, Y. Suganuma, N. Takahashi, J. Sugiyama, Y. Seno, N. L. Yamada, *ACS Appl. Mater. Interfaces* **2016**, *8*, 9540.
[32] M. Steinhauer, M. Stich, M. Kurniawan, B. K. Seidlhofer, M. Trapp, A. Bund, N. Wagner, K. A. Friedrich, *ACS Appl. Mater. Interfaces* **2017**, *9*, 35794.
[33] E. D. Rus, J. A. Dura, *ACS Appl. Mater. Interfaces* **2019**, *11*, 47553.
[34] H. Kiessig, *Ann. Phys.* **1931**, *402*, 769.
[35] J. A. Dura, E. D. Rus, P. A. Kienzle, B. B. Maranville, in *Nanolayer Research* (Ed: T. Imae), Elsevier, Amsterdam **2017**, pp. 155–202.

[36] C. Zhang, Q. Lan, Y. Liu, J. Wu, H. Shao, H. Zhan, Y. Yang, *Electrochim. Acta* **2019**, *306*, 407.
[37] Y. H. Lee, I. C. Leu, S. T. Chang, C. L. Liao, K. Z. Fung, in *Electrochim Acta*, Elsevier Ltd, Amsterdam **2004**, pp. 553–559.
[38] S. Menkin, C. A. O'Keefe, A. B. Gunnarsdóttir, S. Dey, F. M. Pesci, Z. Shen, A. Aguadero, C. P. Grey, *J. Phys. Chem. C* **2021**, *125*, 16719.
[39] M. V. Avdeev, A. A. Rulev, V. I. Bodnarchuk, E. E. Ushakova, V. I. Petrenko, I. V. Gapon, O. V. Tomchuk, V. A. Matveev, N. K. Pleshanov, E. Y. Kataev, L. V. Yashina, D. M. Itkis, *Appl. Surf. Sci.* **2017**, *424*, 378.
[40] J. H. Raberg, J. Vatamanu, S. J. Harris, C. H. M. Van Oversteeg, A. Ramos, O. Borodin, T. Cuk, *J. Phys. Chem. Lett.* **2019**, *10*, 3381.
[41] H. Wang, R. G. Downing, J. A. Dura, D. S. Hussey, in *Polymers for Energy Storage and Delivery: Polyelectrolytes for Batteries and Fuel Cells* (Eds: K. A. Page, C. L. Soles, J. Runt), American Chemical Society, Washington, DC **2012**, pp. 91–106.
[42] D. A. Fischer, G. G. Cohen, N. J. Shevchik, *J. Phys. F Metal Phys.* **1980**, *10*, L139.
[43] J. Stahn, A. Glavic, *Nucl. Instrum. Methods Phys. Res. A* **2016**, *821*, 44.
[44] A. Gibaud, G. Vignaud, S. K. Sinha, *Acta Crystallograph. A* **1993**, *49*, 642.
[45] B. J. Kirby, P. A. Kienzle, B. B. Maranville, N. F. Berk, J. Krycka, F. Heinrich, C. F. Majkrzak, *Curr. Opin. Colloid Interface Sci.* **2012**, *17*, 44.